^{108}Sn studied with intermediate-energy Coulomb excitation

A. Banu,[1,2] J. Gerl,[1] C. Fahlander,[3] M. Górska,[1] H. Grawe,[1] T.R. Saito,[1] H.-J. Wollersheim,[1] F. Nowacki,[4] E. Caurier,[4] A. Gniady,[4] M. Hjorth-Jensen,[5] T. Engeland,[5] T. Beck,[1] F. Becker,[1] P. Bednarczyk,[1,6] M.A. Bentley,[7] A. Bürger,[8] F. Cristancho,[3,†] G. de Angelis,[9] Zs. Dombrádi,[10] P. Doornenbal,[1,11] H. Geissel,[1] J. Gręboszz,[1,6] G. Hammond,[12,‡] M. Hellström,[1,§] J. Jolie,[11] I. Kojouharov,[1] N. Kurz,[1] R. Lozeva,[1,**] S. Mandal,[1,††] N. Mărginean,[9] S. Muralithar,[1,‡‡] J. Nyberg,[13] J. Pochodzalla,[2] W. Prokopowicz,[1,6] P. Reiter,[11] D. Rudolph,[3] C. Rusu,[9] N. Saito,[1] H. Schaffner,[1] D. Sohler,[10] H. Weick,[1] C. Wheldon,[1,§§] and M. Winkler[1]

[1] *Gesellschaft für Schwerionenforschung (GSI), D-64291 Darmstadt, Germany*
[2] *Institut für Kernphysik, Universität Mainz, D-55099 Mainz, Germany*
[3] *Department of Physics, Lund University, S-22100 Lund, Sweden*
[4] *IReS, F-67037 Strasbourg Cedex 2, France*
[5] *Department of Physics and Center of Mathematics for Applications, University of Oslo, N-0316 Oslo, Norway*
[6] *The Henryk Niewodniczański Institute of Nuclear Physics, PAN, 31-342 Kraków, Poland*
[7] *Department of Physics, University of York, Heslington, York YO10 5DD, UK*
[8] *Helmholtz-Institut für Strahlen- und Kernphysik, Universität Bonn, D-53115 Bonn, Germany*
[9] *INFN Laboratori Nazionali di Legnaro, I-35020 Legnaro, Italy*
[10] *Institute of Nuclear Research of the Hungarian Academy of Sciences, H-4001 Debrecen, Hungary*
[11] *Institut für Kernphysik, Universität zu Köln, D-50937 Köln, Germany*
[12] *Department of Physics, University of Keele, Keele, Staffordshire ST5 5BG, UK*
[13] *Department of Radiation Sciences, Uppsala University, SE-75121 Uppsala, Sweden*

(Dated: July 14, 2005)

The unstable neutron-deficient ^{108}Sn isotope has been studied in inverse kinematics by intermediate-energy Coulomb excitation using the RISING/FRS experimental set-up at GSI. This is the highest-Z nucleus studied so far with this method. Its reduced transition probability B(E2;$0^+_{\rm g.s.}\rightarrow 2^+_1$) has been measured for the first time. The extracted B(E2) value of 0.230 (57) e^{2}b^2 has been determined relative to the known value in the stable ^{112}Sn isotope. The result is discussed in the framework of recent large-scale shell model calculations performed with realistic effective interactions. The role of particle-hole excitations of the ^{100}Sn core and of the $Z = 50$ shell gap for the E2 polarization are investigated.

PACS numbers: 21.10.-k, 25.70.De, 23.20.Js, 21.60.Cs

The structure of nuclei far from β-stability is currently a key topic of research, both experimentally and theoretically. The emphasis is put on phenomena such as shell evolution, proton-neutron interaction, and changes of collective properties. A key question in nuclear structure physics is whether the shell closures known close to the valley of stability are preserved when approaching the limits of nuclear existence. Towards the proton drip line due to the confinement of protons by the Coulomb barrier and/or the vicinity of the $N = Z$ line, changes in shell structure as well as collectivity are expected to be driven exclusively by the monopole drift [1, 2] of single-particle states and the proton-neutron interaction between identical shell model orbitals [3]. Hence, core polarization studied in spin (M1, Gamow-Teller) and shape (E2) response, proton-neutron pairing, and isospin symmetry are appealing nuclear structure investigations. In this respect, the heaviest proton bound $N = Z$ doubly-magic nucleus ^{100}Sn and its neighbours provide a principle test ground. Information on quadrupole polarization of the magic core can be inferred from the energy of the first excited 2^+ states and their E2 transition rates to the ground state. Experimentally, the nuclear properties of ^{100}Sn are only indirectly known [4–7], although its existence has already been confirmed [8, 9].

The Sn isotopes between the $N = 50$ and 82 shell closures provide the longest chain of semi-magic nuclei accessible to nuclear structure studies, both in the neutron valence space of a full major shell and with emphasis on excitations of the $Z = 50$ core. The B(E2;$0^+_{\rm g.s.}\rightarrow 2^+_1$)

†On leave of absence from Universidad Nacional de Columbia, Bogota, Columbia
‡Present address: Department of Physics, University of York, Heslington, York, UK
§Present address: Department of Physics, Lund University, Lund, Sweden
**Present address: Faculty of Physics, University of Sofia, Sofia, Bulgaria
††Present address: University of Delhi, New Delhi, India
‡‡Present address: Nuclear Science Center, New Delhi, India
§§Present address: Hahn-Meitner-Institut Berlin, Berlin, Germany

value is most sensitive to details of shell structure and E2 core polarization. The existence of higher lying isomeric states in the tin isotopes hampers a direct measurement of the lifetime of the 2_1^+ states by standard Doppler methods (DSAM, RDM) and the very short lifetimes of the 2_1^+ states are not accessible to electronic timing methods. Therefore, a Coulomb excitation measurement is the only way to obtain this nuclear structure information. Until recently only the $B(E2;0^+_{g.s.}\rightarrow 2_1^+)$ values of the stable $^{112-124}$Sn nuclei were measured in subbarrier Coulomb excitation [10].

In the following, we report on the first intermediate-energy Coulomb excitation experiment performed on the ^{108,112}Sn isotopes using the RISING/FRS set-up [11]. A primary beam of ^{124}Xe at 700 MeV/nucleon energy and an average intensity of 6×10^7 s^{-1}, delivered by the SIS accelerator at GSI, impinged on a 4 g/cm^2 ^{9}Be production target located at the entrance of the fragment separator (FRS) [12]. The tin isotopes were produced via projectile fragmentation. Secondary beams were separated by the FRS operated in achromatic optics mode, and identified on an event-by-event basis by coincidence measurements of energy loss in an ionization chamber, magnetic rigidity, and time-of-flight using two scintillator detectors. The trajectories of the projectiles were tracked with two multiwire proportional chambers. A wedge-shaped aluminium degrader with thickness of 4.59 g/cm^2 and 4.83 g/cm^2 for the ^{108}Sn and ^{112}Sn fragment settings, respectively, was placed at the middle focal plane of the FRS. This allowed an optimized separation of the fragments of interest amounting in both cases to $\simeq 60\%$ of the secondary beam cocktail. At the final focal plane of the fragment separator, a secondary ^{197}Au target was placed with a thickness of 386 mg/cm^2. The ^{108,112}Sn nuclei impinging on the gold target at 142 MeV/nucleon and 147 MeV/nucleon energies, respectively, were mainly excited by means of electromagnetic interaction. Gamma rays in coincidence with projectile residues were detected by the 15 RISING Ge-Cluster detectors [11, 13]. The position sensitive detector array CATE [14], consisting of 3×3 Si-CsI(Tl) modular ΔE-E telescopes, and covering an opening angle of 58 mrad, was placed at 1426 mm downstream from the secondary target. It served for the reaction channel selection as well as for the scattering angle determination.

At intermediate energies, a Coulomb excitation measurement is an experimental challenge because of intense atomic background radiation and relativistic Doppler effects. Previously, the method has been applied to nuclei with $Z \leq 30$ only. The 15 RISING Ge-Cluster detectors were positioned at forward angles with a small opening angle of 3° (for each single crystal) in order to maximize the effective solid angle affected by the Lorentz boost, while at the same time minimizing the Doppler broadening. This allowed an energy resolution of 3% to be achieved for projectile residue velocities of $\cong 0.46c$. To suppress the atomic background radiation, each Ge-Cluster detector was surrounded on the side by a lead sheet of 2 mm thickness, and its front face was shielded by a combination of Pb, Sn and Al absorbers of 5 mm thickness. In the analysis, an add-back procedure (applied to all 7 crystals within a Ge-Cluster) as well as Doppler-shift correction were performed event by event. For technical reasons (see Ref. [15] for details) only five of the RISING Ge-Cluster detectors were suitable for the off-line data analysis. The top panel in Fig. 1 shows the Doppler corrected energy spectrum of the excited ^{112}Sn, with the γ-ray line of interest at 1257 keV. The bottom panel shows the corresponding spectrum for ^{108}Sn with the γ-ray line at 1206 keV.

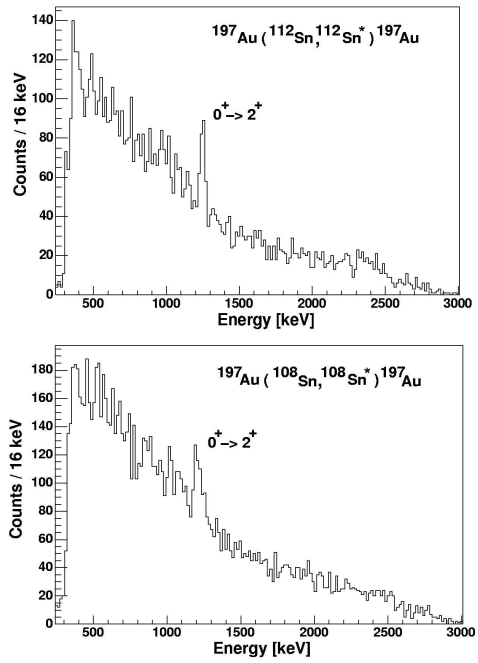

FIG. 1: De-excitation γ-ray lines following $0^+_{g.s.} \rightarrow 2_1^+$ Coulomb excitation of the ^{112,108}Sn projectiles, respectively.

The conditions applied in the data analysis to obtain the spectra in Fig. 1 are the following:
(i) fragment selection before the target with the FRS;
(ii) fragment selection after the target with CATE;
(iii) prompt gamma time 'window' (26 ns wide) selection;
(iv) scattering angle (in the laboratory frame) selection between $1°-2°$;
(v) Ge-Cluster multiplicity $M_\gamma(E_\gamma \geq 500 \text{ keV}) = 1$.
The requested condition on the scattering angle (calculated in the laboratory frame) between $1°-2°$ corresponds approximately to impact parameters in the range 11 to 22 fm [15]. Below this range one expects nuclear interactions to contribute, while above the elastic channel dominates, resulting in increased atomic background.

The intermediate-energy Coulomb excitation reaction is predominantly a *one-step process*, which implies a γ-hit multiplicity equal to one. However, there is a large probability that a de-excitation event is accompanied via

chance coincidences by radiation originating from atomic processes. Therefore, for an appropriate Coulomb excitation event selection, it was required in the analysis that the condition of single γ-hit cluster multiplicity is satisfied only for prompt γ rays at energies in excess of 500 keV (in the laboratory frame). This excluded non-suppressed atomic background radiation produced at the used beam energy.

From the observation of the Doppler corrected γ line corresponding to the $0^+_{\rm g.s.}\rightarrow 2^+_1$ transition in ^{108}Sn, the Coulomb excitation cross section can be extracted, which is directly proportional to the B(E2) value [16]. In the analysis, effects such as particle-γ angular correlations, nuclear excitation or excitations of higher-lying 2^+ states (feeding contributions) have to be considered. These data are not available due to limited statistics. Therefore, we are presenting the experimental result of a relative measurement of the B(E2;$0^+_{\rm g.s.}\rightarrow 2^+_1$) value in ^{108}Sn. The intermediate-energy Coulomb excitation measurement performed on ^{112}Sn with $B(E2; 0^+_{\rm g.s.} \rightarrow 2^+_1) = 0.240\ (14)\ {\rm e^2b^2}$ extracted from a subbarrier Coulomb excitation experiment [10], was used as normalization. This is justified since the two Coulomb excitation experiments were performed under similar conditions. The unknown feeding pattern is thus cancelled out (assuming similar nuclear structure in both ^{108}Sn and ^{112}Sn as supported by theory), as well as the remaining nuclear contribution not removed by the scattering angle condition.
In Table I the experimental parameters needed to calculate the B(E2) value in ^{108}Sn are listed. In addition, information on data-taking time is given for both fragment settings.

TABLE I: The photon yield N_γ, the particle flux on target N_p, and data-taking time for the two ^{108,112}Sn fragment settings.

Isotope	N_γ [a]	N_p [b]	data-taking time
^{108}Sn	174 (26)	15×10^7	58 hrs
^{112}Sn	106 (20)	10×10^7	33 hrs

[a] The photon yield was recorded with γ-particle trigger.
[b] The particle flux on target was inferred from down-scaled particle-singles trigger (see Ref. [15]).

The B(E2;$0^+_{\rm g.s.}\rightarrow 2^+_1$) value in ^{108}Sn was determined as follows

$$B(E2\uparrow)_{108} = B(E2\uparrow)_{112} \times \frac{N_\gamma^{108}}{N_\gamma^{112}} \times \frac{N_p^{112}}{N_p^{108}} \times 0.88,$$

yielding

$$B(E2; 0^+_{\rm g.s.} \rightarrow 2^+_1)_{108} = 0.230\ (57)\ {\rm e^2b^2}.$$

The value 0.88 corresponds to the ratio of the proportionality factors between the excitation cross section and the reduced transition probability for ^{112}Sn and ^{108}Sn. The proportionality factors were calculated with the standard code DWEIKO [17] used for nuclear scattering at intermediate and high energies ($E_{\rm lab} \geqslant 50$ MeV/nucleon), taking into account the scattering angle selection applied in the data analysis. Because the 2^+_1 excited states in ^{108,112}Sn lie close in energy, the same γ-ray efficiency was considered in the B(E2) determination.

In the following, the measured B(E2$\uparrow$) value in the unstable ^{108}Sn is compared to the results of two independent large-scale shell model (LSSM) calculations. The first set of LSSM calculations was performed by the Oslo group for the tin isotopes $^{102-130}$Sn, following the prescription outlined in Ref. [18] and using the CD-Bonn potential for the bare nucleon-nucleon interaction [19]. Two sets of interactions with closed shell cores ^{100}Sn and ^{132}Sn were chosen. The model space for neutrons comprises in both cases the $1d_{5/2}$, $0g_{7/2}$, $1d_{3/2}$, $2s_{1/2}$, and $0h_{11/2}$ orbitals. In the discussion here we focus on the results obtained with the ^{100}Sn closed shell core. A harmonic-oscillator basis was chosen for the single-particle wave functions, with an oscillator energy $\hbar\omega = 8.5$ MeV. The single-particle energies of the chosen model space orbits are $\epsilon_{1d_{5/2}} = 0.00$ MeV, $\epsilon_{0g_{7/2}} = 0.08$ MeV, $\epsilon_{1d_{3/2}} = 1.66$ MeV, $\epsilon_{2s_{1/2}} = 1.55$ MeV, and $\epsilon_{0h_{11/2}} = 3.55$ MeV. The neutron effective charge used in the calculations is $1.0e$. The results of the calculations for the energies of the 2^+_1 excited states and B(E2;$0^+_{\rm g.s.}\rightarrow 2^+_1$) values are presented in columns 3 and 5 of Table II.

In the case of a ^{132}Sn core, the experimental B(E2$\uparrow$) values are reproduced with effective charges between $0.7 - 0.8e$ for all isotopes from ^{120}Sn to ^{130}Sn [20]. For ^{108,112,114}Sn one needs however an effective charge of the order of $1.0e$ to reproduce the experimental values. This indicates that the effective charges for the lighter Sn isotopes show stronger renormalization effects, implying larger core polarization due to particle-hole excitations, and a different character of core excitations in the $N = Z$ and $N >> Z$ regions of the Sn isotopic chain.

In Fig. 2 the systematics of the B(E2$\uparrow$) values in the Sn isotopes ranging from neutron number $N = 50$ to $N = 82$ is shown. The shell-model results used in the systematics in Fig. 2 are taken from the calculation with ^{100}Sn as closed shell core. For comparison the experimental data measured recently for the unstable heavy ^{126,128,130}Sn isotopes [21], the unstable light ^{108}Sn (this work), and the adopted values for the stable tin isotopes $^{112-124}$Sn [10] are shown. The parabola-like trend of the B(E2) systematics resembles the typical behavior of a one-body even tensor operator across a shell in the seniority scheme, which for a seniority changing transition ($\Delta v = 2$) at first increases, then flattens out, peaking at midshell, and falling off thereafter. In a non-unique j shell with many interacting orbitals this can be generalized to B(E2;$0^+_{\rm g.s.}\rightarrow 2^+_1$) $\sim$ f(1$-$f), with f=(N$-$50)/32 the filling factor of the shell, where N denotes the neutron

TABLE II: $I^\pi = 2^+$ energies and E2 strengths in $^{102-130}$Sn.

Isotope	$E_{2_1^+}$ [keV]			B(E2↑) [e^2b^2]	
	Exp.[a]	SM[b]	Exp.	SM[b]	SM[c]
^{102}Sn	1472.0 (2)	1647		0.043	0.044
^{104}Sn	1260.1 (3)	1343		0.094	0.090
^{106}Sn	1207.7 (5)	1231		0.137	0.125
^{108}Sn	1206.1 (1)	1243	0.230 (57)[d]	0.171	0.162
^{110}Sn	1211.9 (2)	1259		0.192	
^{112}Sn	1256.9 (7)	1237	0.240 (14)[a]	0.203	
^{114}Sn	1299.9 (7)	1208	0.24 (5)[a]	0.209	
^{116}Sn	1293.6 (8)	1135	0.209 (6)[a]	0.210	
^{118}Sn	1229.7 (2)	1068	0.209 (8)[a]	0.208	
^{120}Sn	1171.3 (2)	1044	0.202 (4)[a]	0.201	
^{122}Sn	1140.6 (3)	1076	0.192 (4)[a]	0.184	
^{124}Sn	1131.7 (2)	1118	0.166 (4)[a]	0.156	0.174
^{126}Sn	1141.2 (4)	1214	0.10 (3)[e]	0.118	0.134
^{128}Sn	1168.8 (4)	1233	0.073 (6)[e]	0.079	0.090
^{130}Sn	1121.3 (5)	1191	0.023 (5)[e]	0.042	0.047

[a]Ref. [10]
[b]LSSM in a $(g_{7/2}, d, s, h_{11/2})$ neutron space with ^{100}Sn core
[c]LSSM in a proton (g, d, s) and neutron $(g_{7/2}, d, s, h_{11/2})$ model space and a ^{90}Zr core at t=4
[d]this work
[e]Ref. [21]

number [20, 22].

To further investigate the variation and intrinsic *ph* structure of the polarization charge in the pure neutron space, in a second approach the Strasbourg group performed LSSM calculations which allow for proton core excitations [23]. The starting point is the bare nucleon-nucleon interaction of the Oslo group, phenomenologically adjusted to the spectroscopy of Sn isotopes and $N = 82$ isotones. The differences consist in choosing ^{90}Zr as closed shell core, and consequently a different model space including protons, namely $0g_{9/2}$, $0g_{7/2}$, $1d_{5/2}$, $1d_{3/2}$ and $2s_{1/2}$. For the neutrons the same model space as for the first set was used. The calculations allow up to 4p-4h proton core excitations, and the effective charges are set to $1.5e$ and $0.5e$ for protons and neutrons, respectively. Since the chosen model space is rather large, the coupled scheme code NATHAN is used [24]. In addition, a seniority truncation is applied. In these calculations at the computational limits results close to convergence are obtained for seniority up to 8.

The experimentally observed dissymmetry of the B(E2) systematics, supported also by recent preliminary results on ^{110}Sn measured at REX-ISOLDE [25], suggests to study the role of proton core excitations and the evolution of the Z=50 shell gap. The proton-neutron interaction plays here an essential role. In particular the $\pi(0g_{9/2}) - \nu(0g_{7/2}1d_{5/2}1d_{3/2}2s_{1/2})$ monopoles, responsable for the evolution of the spectroscopy between ^{91}Zr and ^{101}Sn, govern the evolution of the proton $Z = 50$ gap with the neutron filling. The tuning of the interaction for ^{91}Zr and ^{101}Sn is therefore sufficient to maintain the experimental $Z = 50$ shell gap as extracted from mass measurements.

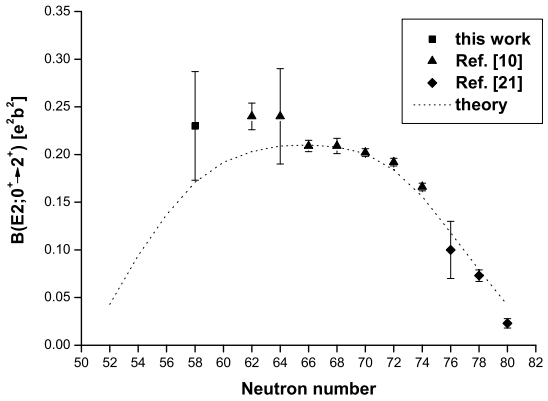

FIG. 2: Measured B(E2;$0^+_{\rm g.s.} \rightarrow 2^+_1$) values and theoretical predictions in the full $N = 50 - 82$ neutron space (see text).

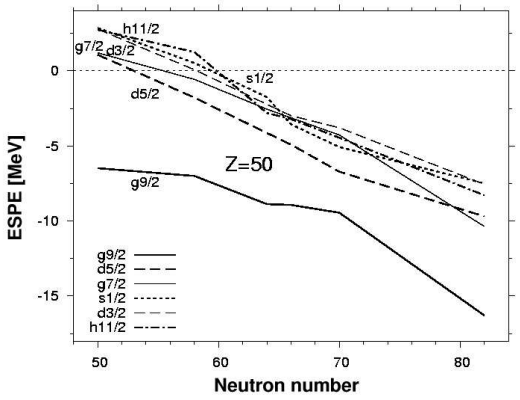

FIG. 3: Calculated evolution of the proton ESPE with the neutron number N along the chain of Sn isotopes.

This is reflected in Fig. 3 for the proton Effective Single Particle Energies (ESPE), as defined in Ref. [1], along the tin chain. Note that the ESPEs shown are not identical with the experimentally observed single particle states, which comprise configuration mixing and are well reproduced by the full shell model calculations. In particular, Fig. 3 shows the crossing for the ESPE of the $1d_{5/2}$ and $0g_{7/2}$ orbitals due to a strong $g_{7/2} - h_{11/2}$ proton-neutron monopole and the parallel behaviour of the $0g_{9/2}$ and $0g_{7/2}$ orbitals so that a sufficiently closed ^{132}Sn is maintained.

The trend of the B(E2) curve can thus be explained by the reduction of the effective proton gap towards midshell Sn isotopes. The B(E2) systematics presented in Fig. 4 compares the aforementioned experimental values [10, 15, 21] with theoretical predictions when proton $np - nh$ core excitations ($t = n$) are considered.

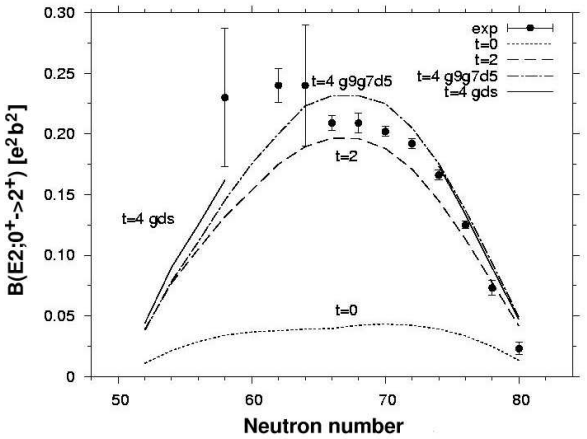

FIG. 4: Comparison of measured B(E2↑) values with LSSM predictions by taking into account *ph* core excitations. The $t = 0$ curve corresponds to Fig 2. The $t = 2$ curve shows the major contribution as given by proton core excitations. The $t = 4$ curves are shown for the whole tin chain in a truncated proton model space and untruncated in the *gds* major shell.

It is interesting to notice that the untruncated proton 4p-4h core excitations (listed also in the last column of Table II) show no increase, but rather a small decrease in the B(E2) strength for the heavy tin isotopes in comparison to the case of the $t = 4$ truncated to the $0g_{9/2}, 0g_{7/2}, 1d_{5/2}$ orbitals, whereas for the light ones a substantial increase is observed. This would explain the aforementioned dissymmetry in the trend of measured B(E2) values. The truncated $t = 4$ calculations already seem to overestimate the strength by about 15%, which can be ascribed to an ambiguity in the $\pi(0g_{9/2}) - \nu(1h_{11/2})$ monopole due to experimental uncertainties in the $11/2^-$ states in $N = 51$ nuclei. A slight increase would open the $Z = 50$ shell gap in the heavier Sn isotopes and, hence, reduces the B(E2) values. However, a more detailed discussion of the midshell and heavy Sn isotopes is beyond the scope of the present work and will be discussed in a forthcoming paper [23]. Moreover, it can be expected from recent work in ^{98}Cd [5] that an extension to higher t, which exceeds the present computational limits, will further increase the E2 strength for the neutron-deficient Sn isotopes.

In conclusion, the B(E2;$0^+_{\rm g.s.}\rightarrow 2^+_1$) value in the unstable ^{108}Sn isotope was measured for the first time by intermediate-energy Coulomb excitation. This is the highest-Z nucleus studied with this method. The comparison with two different but complementary large-scale shell model calculations shows agreement with experiment and gives insight into the microscopic structure of the neutron E2 polarization charge. The evolution of proton ESPE and the $Z = 50$ shell gap with increasing occupation of the N=50-82 major neutron shell govern the dissymmetric trend of the E2 core polarization. The successful B(E2) measurement on ^{108}Sn at GSI opens the research path to study the lighter Sn isotopes via intermediate-energy Coulomb excitation towards ^{100}Sn.

We thank the GSI accelerator staff for their efforts to produce a good quality primary ^{124}Xe beam and the DVEE division at GSI for their support in data acquisition and Go4 software. This work was supported by the BMBF under contracts 06MZ176 and 06-K-167.

REFERENCES

[1] T. Otsuka *et al.*, Phys. Rev. Lett. **87**, 082502 (2001).
[2] H. Grawe, in *The Euroschool Lectures on Physics with Exotic Beams, Vol.I*, Lect. Notes Phys. **651** (Springer, Berlin Heidelberg, 2004), p. 33.
[3] W. Nazarewicz, J. Dobaczewski, and T.R. Werner., Physica Scripta T **56**, 9, (1995).
[4] M. Górska *et al.*, Phys. Rev. Lett. **79**, 2415 (1997).
[5] A. Blazhev *et al.*, Phys. Rev. C **69**, 64304 (2004).
[6] M. Lipoglavšek *et al.*, Phys. Lett. B **440**, 246 (1998).
[7] M. Górska *et al.*, Phys. Rev. C **58**, 108 (1998).
[8] M. Lewitowicz *et al.*, Phys. Lett. B **332**, 20 (1994).
[9] R Schneider *et al.*, Z. Phys. A **348**, 241 (1994).
[10] S. Raman, C.W. Nestor, and P. Tikkanen, At. Data Nucl. Data Tables **78**, 42 (2001).
[11] H.J. Wollersheim *et al.*, Nucl. Instrum. Methods Phys. Res. A **537**, 637 (2005).
[12] H. Geissel *et al.*, Nucl. Instrum. Methods Phys. Res. B **70**, 286 (1992).
[13] J. Simpson, Z. Phys. A **358**, 139 (1997).
[14] R. Lozeva *et al.*, Acta Phys. Pol. **B36**, 1245 (2005).
[15] A. Banu, Ph.D. thesis (2005), University of Mainz.
[16] A. Winther and K. Alder, Nucl. Phys. **A319**, 518 (1979).
[17] C.A. Bertulani, C.M. Campbell, and T. Glasmacher, Comput. Phys. Commun. **152**, 317 (2003).
[18] M. Hjorth-Jensen, T.T.S. Kuo, and E. Osnes, Phys. Rep. **261**, 125 (1995).
[19] R. Machleidt, F. Sammarruca, and Y. Song, Phys. Rev. C **53**, 1483 (1996).
[20] A. Holt, T. Engeland, M. Hjorth-Jensen, and E. Osnes, Nucl. Phys. **A634**, 41 (1998).
[21] D.C. Radford *et al.*, Nucl. Phys. **A746**, 83c (2004).
[22] I. Talmi, Proc. Int. School "Enrico Fermi", *Elementary Modes of Excitation in Nuclei*, ed. A. Bohr and R.A. Broglia (North Holland, Amsterdam, 1977) p.352.
[23] A. Gniady *et al.* (to be published).
[24] E. Caurier and G. Martínez-Pinedo, Nucl. Phys. **A704**, 60c (2002).
[25] J. Cederkäll *et al.* (to be published).